JBC RESEARCH ARTICLE

The CTP-binding domain is disengaged from the DNA-binding domain in a cocrystal structure of *Bacillus subtilis* Noc–DNA complex

Received for publication, January 12, 2023, and in revised form, February 15, 2023 Published, Papers in Press, February 23, 2023,
https://doi.org/10.1016/j.jbc.2023.103063

Kirill V. Sukhoverkov[1,‡], Adam S. B. Jalal[1,2,‡], James R. Ault[3], Frank Sobott[3], David M. Lawson[4], and Tung B. K. Le[1,*]

From the [1]Department of Molecular Microbiology, John Innes Centre, Norwich, United Kingdom; [2]Section of Structural and Synthetic Biology, Department of Infectious Diseases, Faculty of Medicine, Imperial College London, London, United Kingdom; [3]Astbury Centre for Structural Molecular Biology, School of Molecular and Cellular Biology, University of Leeds, Leeds, United Kingdom; [4]Department of Biochemistry and Metabolism, John Innes Centre, Norwich, United Kingdom

Reviewed by members of the JBC Editorial Board. Edited by Ursula Jakob

In *Bacillus subtilis*, a ParB-like nucleoid occlusion protein (Noc) binds specifically to Noc-binding sites (*NBSs*) on the chromosome to help coordinate chromosome segregation and cell division. Noc does so by binding to CTP to form large membrane-associated nucleoprotein complexes to physically inhibit the assembly of the cell division machinery. The site-specific binding of Noc to *NBS* DNA is a prerequisite for CTP-binding and the subsequent formation of a membrane-active DNA-entrapped protein complex. Here, we solve the structure of a C-terminally truncated *B. subtilis* Noc bound to *NBS* DNA to reveal the conformation of Noc at this crucial step. Our structure reveals the disengagement between the N-terminal CTP-binding domain and the *NBS*-binding domain of each DNA-bound Noc subunit; this is driven, in part, by the swapping of helices 4 and 5 at the interface of the two domains. Site-specific crosslinking data suggest that this conformation of Noc-*NBS* exists in solution. Overall, our results lend support to the recent proposal that *parS/NBS* binding catalyzes CTP binding and DNA entrapment by preventing the reengagement of the CTP-binding domain and the DNA-binding domain from the same ParB/Noc subunit.

Cells must couple chromosome segregation and division to reproduce efficiently. In Firmicutes, such as *Bacillus subtilis*, the nucleoid occlusion protein Noc contributes to the coordination between chromosome segregation and the initiation of cell division (1–4). Noc helps direct the assembly of the cell division machinery towards the middle of a dividing cell where the concentration of DNA is the least, thus increasing cell division efficiency (2–4). Critical to this function of Noc is its ability to recruit chromosomal DNA to the cell membrane to form large Noc–DNA-membrane complexes, which inhibit the FtsZ-ring formation over the nucleoid and/or to corral the FtsZ ring towards the mid-cell position (5, 6). Noc is a paralog of a chromosome partitioning protein ParB and is also a CTPase enzyme that binds CTP to form a protein clamp that can slide and entrap DNA (6–8). Apo-Noc first binds to nucleate on 16-bp Noc-binding sites (*NBSs*) scattered along the chromosome (6, 9, 10). The nucleation at *NBS* promotes CTP binding and the subsequent engagement of N-terminal domains from opposing subunits of a Noc homodimer to form a clamp-closed complex that can escape from *NBS* to slide and spread to the neighboring DNA while still entrapping DNA (6). The DNA-entrapped Noc–CTP complexes are also active at binding to the cell membrane due to the liberation of a 10-amino-acid membrane-targeting amphipathic helix (6). As a result, Noc-CTP brings the entrapped chromosomal DNA close to the cell membrane to form large Noc–DNA-membrane complexes that are inhibitory to the assembly of nearby cell division machinery (5, 6).

We previously solved two X-ray crystallography structures of the CTP-binding domain and DNA-binding domain of a *Geobacillus thermoleovorans* Noc to understand the molecular mechanism of this protein family (6). Nevertheless, it remains unclear how the Noc-*NBS*–binding event mechanistically promotes the N-terminal domain engagement to form a closed-clamp Noc. To investigate further, in this study, we solve a structure of a C-terminally truncated *B. subtilis* Noc in complex with *NBS* DNA to reveal the conformation of a nucleating Noc. Through comparisons to other available structures of Noc, and its paralog ParB, and by in-solution site-specific crosslinking, we provide evidence for the extended conformation of nucleating Noc.

Results

Cocrystal structure of a truncated B. subtilis *Noc with* NBS *DNA reveals that the N-terminal CTP-binding domain of each Noc subunit is disengaged from its DNA-binding domain*

To gain insight into the nucleating state of Noc, we employed hydrogen-deuterium exchange coupled to mass spectrometry (HDX-MS) to measure the exchange of amide hydrogen atoms with deuterium atoms in the solvent between *B. subtilis* apo-Noc and *NBS*-bound Noc (Fig. S1). The area of

‡ These authors contributed equally to this work.
* For correspondence: Tung B. K. Le, tung.le@jic.ac.uk.

protection, which is indicative of the *NBS*-binding area, spans the central region of Noc protein from residues 128 to 224. The rest of Noc shows little to no difference in exchange of deuterium between the apo- and *NBS*-bound state (Fig. S1). Next, we sought to determine a cocrystal structure of a *B. subtilis* Noc–*NBS* complex to investigate Noc–*NBS* interaction at a higher resolution. To facilitate crystallization, we engineered a NocΔCTD variant that lacks the flexible 41-amino-acid C-terminal domain (CTD) (Fig. 1*A*). This CTD shows insignificant difference in deuterium exchange between apo-Noc and *NBS*-bound Noc (Fig. S1) and is mostly responsible for Noc dimerization (5, 6). After screening NocΔCTD with several *NBS* duplexes of various lengths, we solved a 2.9 Å resolution cocrystal structure of NocΔCTD with 16-bp *NBS* DNA (see Experimental procedures) (Table 1) (Fig. 1, *A* and *B*). The asymmetric unit (ASU) contains two copies of NocΔCTD bound to a single 16-bp *NBS* DNA duplex (Fig. 1*B*). Together with HDX-MS data, we assigned two domains to each NocΔCTD subunit: an N-terminal CTP-binding domain (NTD) (helices α1 to 4 and sheets β1 to 4) and an *NBS* DNA-binding domain (DBD) (helices α5 to 11) (Fig. 1*C*). The electron density for the first 27 amino acids that contains the membrane-targeting peptide was poorly resolved, and thus this region is absent from the model (Fig. 1*A*). Each NocΔCTD subunit is bound to a half *NBS* site; the *NBS* DNA adopts a conformation whereby in one strand the 5′ base was flipped out, and in the other, the 3′ base was flipped out, enabling a sticky-ended interaction (with a one-base overhang) between the duplexes in adjacent ASUs (Figs. 1*B* and S2). The flipped-out bases are not part of the core 14-bp Noc-binding site (10), thus they are unlikely to contribute to the binding specificity between Noc and DNA.

We previously solved a structure of only the DBD of Noc with *NBS* (2.23 Å, PDB: 6Y93) to elucidate the molecular basis for *NBS*-binding specificity (10). Given that the conformation of the DBD and the core *NBS* site are similar between the previous structure and the structure in this work (RMSD = 0.46 Å), we describe the conformation of the NTD in-depth here instead. By structural alignment of the two NocΔCTD subunits, we noted that the DBD and helices α4-5 are highly similar (RSMD = 0.27 Å), while the rest of the NTD (β1-β4) is orientated in a different direction (approx. 30° apart, owing to the flexible loop in between α4 and β4) (Fig. 2*A*). The multiple alternative orientations at the NTD are likely a common feature of all nucleating ParB family proteins, including Noc. This was the case for the NTD of *Caulobacter crescentus* ParB bound to *parS* DNA (11) and is also evidential from the superimposition of the *B. subtilis* NocΔCTD-*NBS* structure onto that of ParBΔCTD-*parS* from *Helicobacter pylori* and *C. crescentus* (Fig. 2*B*) (11, 12). Multiple alternative conformations of nucleating ParB/Noc family members suggest flexibility at the N-terminal CTP-binding domain.

The most notable feature of the NocΔCTD-*NBS* structure is the disengagement of the NTD and DBD (Fig. 1*C*), which is likely driven by the swinging-out conformation of α4-α5 (Fig. 3, *A* and *B*). Helices α4 and α5 from the same NocΔCTD

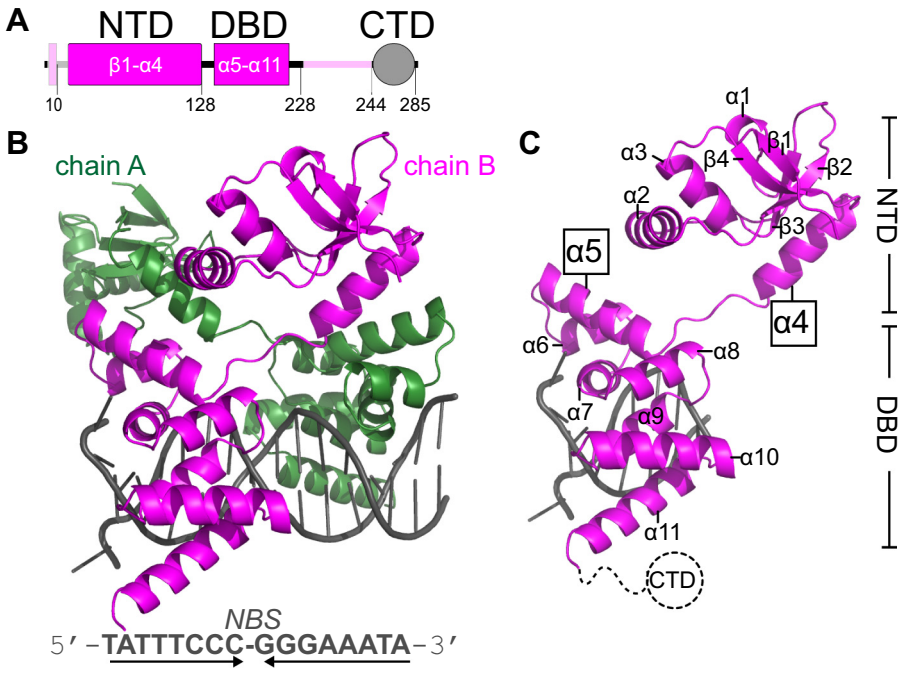

Figure 1. Cocrystal structure of *Bacillus subtilis* Noc with *NBS* DNA reveals that the N-terminal CTP-binding domain of each Noc subunit is disengaged from its DNA-binding domain. *A*, the domain architecture of *B. subtilis* Noc: the 10-amino-acid N-terminal membrane-targeting peptide, the N-terminal CTP-binding domain (NTD), the central DNA-binding domain (DBD), and the C-terminal domain (CTD). Segments of Noc that are not observed in the structure of NocΔCTD-*NBS* DNA are shown in *pale magenta*. The CTD (*gray*) was truncated from Noc to facilitate crystallization. *B*, cocrystal structure of two NocΔCTD subunits (chain A: *dark green*, chain B: *magenta*) bound to a 16-bp *NBS* DNA duplex (*gray*). The nucleotide sequence of a 16-bp *NBS* is shown below the crystal structure; *converging arrows* indicate that *NBS* is palindromic. *C*, the structure of chain B of NocΔCTD (*magenta*) bound to an *NBS* half-site with key features such as the swinging-out helices α4-α5 is highlighted. CTD, C-terminal domain; *NBS*, Noc-binding site; Noc, nucleoid occlusion protein.

Table 1
X-ray data collection, processing, and refinement statistics

Data collection	
Diamond Light Source beamline	I04
Wavelength (Å)	0.979
Detector	Eiger2 XE 16M
Resolution range (Å)	70.27–2.90 (3.08–2.90)
Space Group	$P2_12_12_1$
Cell parameters (Å)	a = 70.5, b = 99.3, c = 99.4
Total no. of measured intensities	164,414 (27,117)
Unique reflections	16,090 (2546)
Multiplicity	10.2 (10.7)
Mean $I/\sigma(I)$	11.7 (1.2)
Completeness (%)	100.0 (100.0)
R_{merge}[a]	0.097 (1.976)
R_{meas}[b]	0.102 (2.076)
$CC_{½}$[c]	0.999 (0.691)
Wilson B value (Å^2)	85.6
Refinement	
Resolution range (Å)	70.27–2.90 (2.98–2.90)
Reflections: working/free[d]	15,216/1101
R_{work}[e]	0.230 (0.407)
R_{free}[e]	0.278 (0.419)
Ramachandran plot: favored/allowed/disallowed[f] (%)	96.5/3.5/0
R.m.s. bond distance deviation (Å)	0.003
R.m.s. bond angle deviation (°)	1.18
Mean B factors: protein/DNA/overall (Å^2)	123/86/117
PDB accession code	7OL9

Values in parentheses are for the outer resolution shell.
[a] $R_{merge} = \sum_{hkl}\sum_i |I_i(hkl) - \langle I(hkl)\rangle| / \sum_{hkl}\sum_i I_i(hkl)$.
[b] $R_{meas} = \sum_{hkl}[N/(N-1)]^{1/2} \times \sum_i |I_i(hkl) - \langle I(hkl)\rangle| / \sum_{hkl}\sum_i I_i(hkl)$, where $I_i(hkl)$ is the ith observation of reflection hkl, $\langle I(hkl)\rangle$ is the weighted average intensity for all observations i of reflection hkl, and N is the number of observations of reflection hkl.
[c] $CC_{½}$ is the correlation coefficient between symmetry equivalent intensities from random halves of the dataset.
[d] The dataset was split into "working" and "free" sets consisting of 95 and 5% of the data, respectively. The free set was not used for refinement.
[e] The R-factors R_{work} and R_{free} are calculated as follows: $R = \sum(|F_{obs} - F_{calc}|)/\sum|F_{obs}|$, where F_{obs} and F_{calc} are the observed and calculated structure factor amplitudes, respectively.
[f] As calculated using MolProbity (30).

subunit are not packed together, instead α4 swings outward by approx. 100° to pack against α5′ from the adjacent NocΔCTD subunit (Fig. 3*A*). This swinging-out conformation has not been observed in the previous structures of DNA-bound *C. crescentus* or *H. pylori* ParBΔCTD, *Thermus thermophilus* ParBΔCTD-apo, or *G. thermoleovorans* NocΔCTD-apo (Figs. 3*B* and S3) (6, 11–13). In previous structures of apo- or DNA-bound ParB/Noc, the equivalent helix α4 consistently folds back to pack with α5 from the same protein subunit (the folding-back conformation) (Figs. 3*B* and S3). The swinging-out conformation of helices α4-5 is often associated with the nucleotide-bound state of ParB/Noc instead (Figs. 3*B* and S3) (6, 7, 11, 14). It has been suggested that CTP binding most likely facilitates the swinging-out conformation of ParB/Noc since nucleotides have been observed to make numerous contacts to both the equivalent α4 and the α4-α5 connecting loop in various ParB proteins (7, 8, 11, 14). The observation of a swinging-out conformation in DNA-bound Noc is therefore surprising, given that CTP was not included in the crystallization drop and that CTP binding is incompatible with high-affinity binding at the nucleation site *NBS* (6). We reason that the swinging-out conformation might be thermodynamically possible in the DNA-bound nucleating ParB/Noc and that CTP binding, instead of facilitating, further stabilizes this swinging-out conformation.

*Site-specific cysteine-cysteine crosslinking suggests the swinging-out conformation of Noc-*NBS *in solution*

To test if the swinging-out conformation of α4-α5 is possible in *NBS*-bound Noc in solution, we employed site-specific chemical crosslinking with the cysteine-specific compound bismaleimidoethane (BMOE) (15). Based on the structures of apo-NocΔCTD (6) and NocΔCTD-*NBS*, we engineered a dual cysteine substitution at E112 and H143 on an otherwise cysteine-free *B. subtilis* Noc to create a Noc (E112C H143C) variant (Fig. 3*A*). In the folding-back conformation where helices α4 and α5 from the same Noc subunit pack together, crosslinking of E112C to H143C would generate an intramolecular crosslinked species (Noc IntraXL), while a swinging-out conformation would give rise to intermolecularly crosslinked species (a singly-crosslinked Noc InterXL and a doubly-crosslinked Noc Inter2XL) which are twice the theoretical molecular weight of a Noc monomer (Fig. 4*A*). Crosslinking of apo-Noc (E112C H143C) only resulted in a prominent band that migrated faster in a denaturing acrylamide gel than noncrosslinked protein (Fig. 4*B*, lane 1 *versus* 2); this is most likely a Noc IntraXL species. Little of Noc InterXL or Inter2XL species was observed (∼4.4% crosslinked fraction), suggesting that the swinging-out conformation is unfavored in apo-Noc (Fig. 4*B*, lane 1 *versus* lane 2). The addition of only CTP did not promote the swinging-out conformation noticeably (Fig. 4*B*, lane 2, ∼4.4% *versus* lane 4, ∼8.7% crosslinked fraction). The singly (InterXL) and the doubly (Inter2XL) crosslinked species appeared more prominently when *NBS* only (Fig. 4*B*, lane 2, ∼4.4% *versus* lane 3, ∼19.3% crosslinked fraction) or *NBS* + CTP were preincubated with Noc (Fig. 4*B*, lane 2, ∼4.4% *versus* lane 5, ∼31.5% crosslinked fraction). The InterXL/2XL fraction further increased, up to ∼37% crosslinked fraction, when *NBS* was used in a molar excess to Noc (E112C H143C) (Fig. S4). We were able to assign different bands to either being InterXL or Inter2XL by performing crosslinking reactions of Noc (E112C H143C) + *NBS* + CTP with an increasing concentration of the BMOE crosslinker (Fig. 4*C*). The assumption is that a singly-crosslinked InterXL preferably forms at a lower concentration of a crosslinker. Overall, our result suggests that the swinging-out conformation of α4-5 exists in solution and is promoted when Noc is bound to the *NBS* DNA.

Discussion

In *B. subtilis*, *noc* resulted from *parB via* a gene duplication and neo-functionalization event (10, 16), and both Noc and ParB are CTP-dependent molecular switches (7, 8, 17–20). CTP-binding switches nucleating ParB/Noc (bound at a high-affinity *parS*/*NBS* site) from an open-clamp conformation (Fig. 5, *A* and *B*) to a closed-clamp conformation that can escape from *parS*/*NBS* to slide to neighboring DNA while still entrapping DNA (Fig. 5*C*) (6, 7, 14, 17, 18). The closed-clamp conformation is possible due to the new dimerization interface between the two adjacent N-terminal CTP-binding domains of ParB/Noc (the so-called NTD-NTD engagement, Fig. 5*C*) (6, 7, 14, 15, 17). Here, our NocΔCTD-*NBS* structure

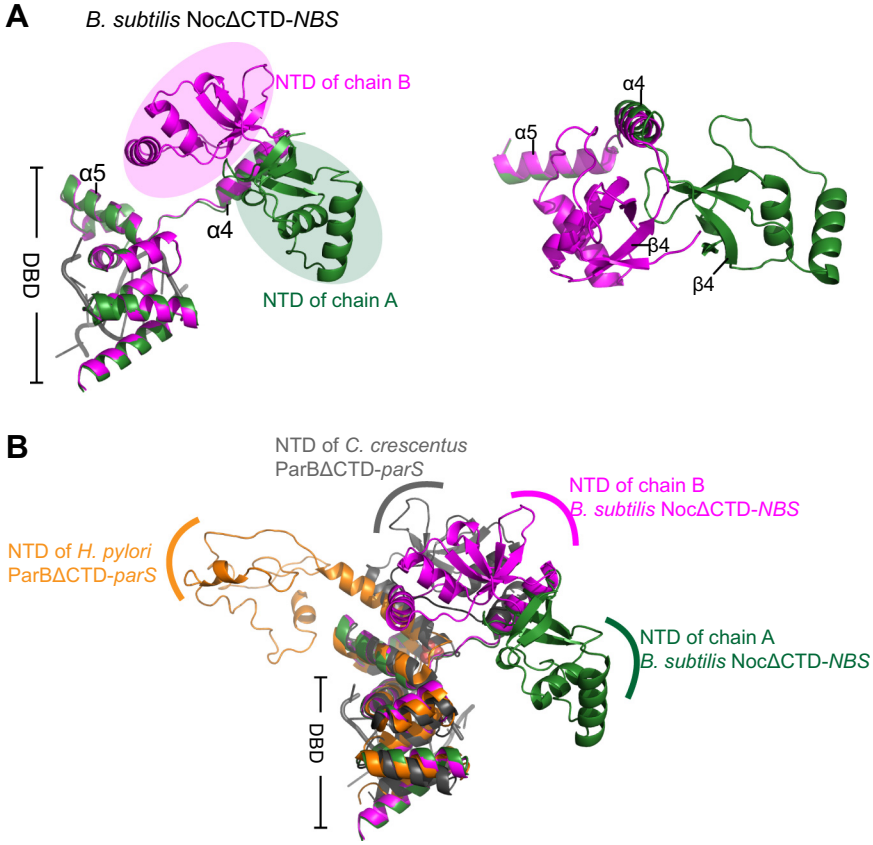

Figure 2. Co-crystal structure of *Bacillus subtilis* NocΔCTD-*NBS* shows alternative orientations at the N-terminal domain (NTD) of Noc. *A*, *left panel*, superimposition of chain A and chain B of NocΔCTD shows the different orientations of the NTD. *Right panel*, the *top-down* view of the superimposition of NocΔCTD subunits shows the majority of the NTD orientates ∼30° apart; part of the DBD (from α6 to α11) was omitted for clarity. Half of the 16-bp palindromic *NBS* site (*gray*) is shown. *B*, structural superimposition of *B. subtilis* NocΔCTD-*NBS* upon other available DNA-bound ParB structures highlights the variation in the orientation of the NTD. CTD, C-terminal domain; DBD, DNA-binding domain; *NBS*, Noc-binding site; Noc, nucleoid occlusion protein; NTD, N-terminal domain; ParB, Partitioning protein B.

represents an open-clamp conformation because there is no protein-protein contact between the majority of two adjacent NTDs of Noc, except for the swapping helices α4 and α4' (Figs. 1*B* and 5*B*).

It has been observed that, without *parS*/*NBS*, CTP is unable to efficiently promote the NTD-NTD engagement to close the ParB/Noc clamp (6, 7, 14, 17). To rationalize this phenomenon, Antar *et al.* (15) noted that two ParB subunits would not be able to occupy a *parS* site if they were to adopt a conformation similar to apo-ParB (in which the NTD and the DBD of the same ParB subunit fold back on each other) because of a severe clash between opposing ParB subunits. Antar *et al.* (2021) (15) proposed that, to avoid this potential clash, the NTD and the DBD from each *parS*-bound ParB must be untethered/disengaged from each other. The DBD-NTD disengagement later favors the two opposing NTDs to dimerize in the presence of CTP to form a clamp-closed complex (15). In sum, *parS* serves as a catalyst in a reaction that favors the formation of the product (the closed clamp) by inhibiting the reversion to the substrate (the open clamp apo-ParB). Our structure of DNA-bound Noc here lends support to this hypothesis because the conformation of the DNA-bound Noc subunit is drastically different from that of apo-Noc, especially with the swinging-out helices α4-α5 disengaging the NTD and DBD from each other (Fig. 5B_i). It is possible that *NBS*-bound Noc might exist as an ensemble of states with helices α4-α5 in either a folding-back (Fig. 5B_{ii}) or a swinging-out conformation (Fig. 5B_i) and that the NocΔCTD-*NBS* structure here represents a snapshot of this dynamic process. The swinging-out conformation of α4-α5 might be rare in solution, given that the crosslinking reaction of Noc (E112C H143C) + *NBS* produced IntraXL as the major species. Nevertheless, the proportion of InterXL and Inter2XL increased substantially when *NBS* (Fig. 4*B*, lane 3) is included in comparison to apo-Noc only (lane 2) or Noc + CTP only conditions (lane 4). Moreover, the proportion of InterXL and Inter2XL also increased when *NBS* was added in excess (Fig. S4). The proximity of adjacent Noc subunits and the restriction in movement by a DNA-fixated DBD may increase the likelihood of swapping helices α4-α5 in Noc. This might in part contribute to further promoting the NTD-NTD engagement upon CTP binding (Fig. 5*C*) and might additionally explain how *NBS* serves as a catalysis for NTD-NTD engagement and thus clamp closure for a ParB-like protein Noc. However, it is also worth noting that ParB, in the presence of *parS*, does not undergo α4-α5 swapping as readily as Noc-*NBS* (S. Gruber, personal communication) (15). It is still unclear why this is the case and how it is related to the biological

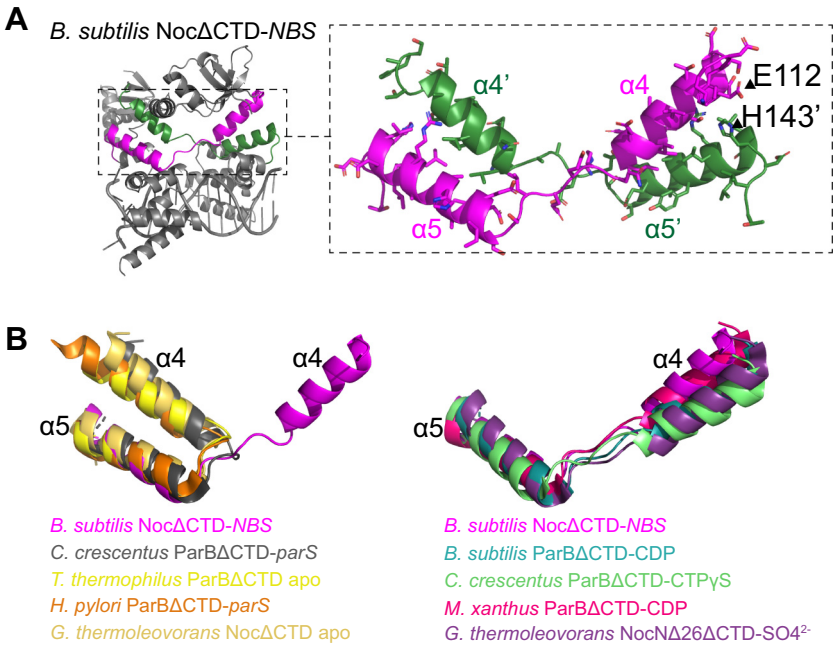

Figure 3. Helices α4-α5 from the *Bacillus subtilis* NocΔCTD–*NBS* complex adopt a swinging-out conformation. *A*, cocrystal structure of *B. subtilis* NocΔCTD with *NBS* (*left panel*) with the pairs of swapping helices (α4-α5 and α4′-α5′ for the opposite subunit) highlighted in *magenta* and *dark green*, respectively (*right panel*). Amino acid side chains of α4-α5 and α4′-α5′ are shown in *stick* representation to illustrate the packing between helices from opposite Noc subunit. The positions of residues E112 (on α4) and H143 (on α5), which were substituted for cysteine in a crosslinking assay (Fig. 4), are also shown. *B*, superimposition of the helices α4-α5 from *B. subtilis* NocΔCTD–*NBS* complex upon the equivalent pair of helices in other apo-ParB/Noc or DNA-bound ParB structures (*left panel*) or upon the equivalent pair of helices in other nucleotide-bound ParB/Noc structure (*right panel*). The *Geobacillus thermoleovorans* NocNΔ26ΔCTD-$SO4^{2-}$ structure is thought to represent the conformation of Noc in a nucleotide-bound state as the sulfate anion from crystallization solution occupies a position equivalent to that of the β-phosphate moiety of CTP (6). CTD, C-terminal domain; *NBS*, Noc-binding site; Noc, nucleoid occlusion protein; ParB, Partitioning protein B.

functions of ParB *versus* Noc, but it might explain why helices α4-α5 in all previous X-ray crystallography structures of ParB-*parS* complex are all in the folding-back conformation (11, 12).

Experimental procedures

Plasmid and strain construction

Construction of pET21b:: Bacillus subtilis NocΔCTD-his$_6$ and pET21b::noc (E112C H143C)-his$_6$

The coding sequence of a 41-amino-acid C-terminally truncated *B. subtilis* Noc was amplified by PCR using a forward primer (AACTTTAAGAAGGAGATATACATATGAAGCATTCATTCTCTCGTTTCTTC) and a reverse primer (GTGGTGCTCGAGTGCGGCCGCAAGCTTATCTCTGCTGAATGCTTTGCGTCTC) and pET21b::*B. subtilis* Noc-his$_6$ (6) as template. The resulting PCR product was gel-purified and assembled into an NdeI-HindIII-cut pET21b using a 2× Gibson master mix (NEB). Gibson assembly was possible owing to a 23-bp sequence shared between the NdeI-and-HindIII cut pET21b backbone and the PCR amplified fragment. The 23-bp homologous region was introduced during the synthesis of the above primers.

A dsDNA fragment containing a *B. subtilis noc (E112C H143C)* gene was chemically synthesized (gBlocks, IDT). The gBlocks fragment was assembled into an NdeI-HindIII-cut pET21b using a 2× Gibson master mix to result in *pET21b::noc (E112C H143C)-his$_6$*. All plasmids were verified by Sanger sequencing (Eurofins).

Protein overexpression and purification

B. subtilis Noc (WT)-His_6 and *B. subtilis* NocΔCTD-His_6 were purified through a 3-column (HisTrap, Heparin, Superdex-75 gel filtration) procedure as described previously (6). Purified NocΔCTD-His_6 was stored at −80 °C in storage buffer (10 mM Tris–HCl pH 8.0 and 250 mM sodium chloride) before crystallization.

Noc (E112C H143C)-His_6 was purified using a His-Select Cobalt Affinity gel and subsequently Superdex-200 gel filtration, using the following buffers: buffer A-HisTrap (100 mM Tris–HCl pH 7.4, 300 mM sodium chloride, 10 mM imidazole, 5% (v/v) glycerol), buffer B-HisTrap (100 mM Tris–HCl pH 7.4, 300 mM sodium chloride, 500 mM imidazole, 5% (v/v) glycerol), and gel filtration buffer (100 mM Tris–HCl pH 7.4 and 300 mM sodium chloride). Purified protein was concentrated using an Amicon Ultra-4 10 kDa cut-off spin column and stored at −80 °C in storage buffer (100 mM Tris–HCl pH 7.4, 300 mM sodium chloride, 10 (v/v) glycerol, and 0.1 mM Tris(2-carboxyethyl)phosphine).

In vitro *crosslinking using a sulfhydryl-to-sulfhydryl crosslinker BMOE*

Noc (E112C H143C)-His_6 (4 μM final concentration) was incubated on ice either alone or with 1 mM CTP, or 1 μM 22-bp *NBS* DNA duplex (or with a twofold increasing concentration of *NBS* from 0 to 5 μM), or both in a crosslinking buffer (100 mM Tris–HCl pH 7.4, 130 mM sodium chloride,

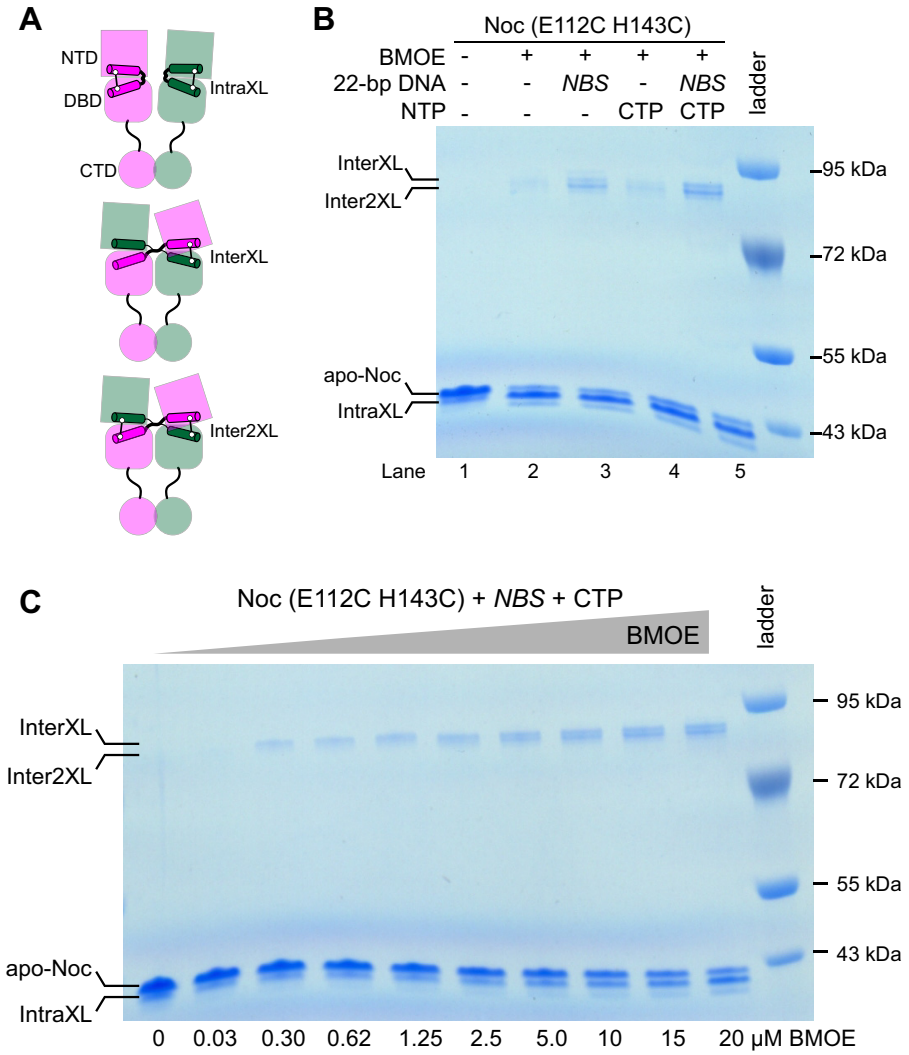

Figure 4. Site-specific crosslinking of *Bacillus subtilis* Noc (E112C H143C) suggests that the swinging-out conformation of Noc-*NBS* exists in solution. *A*, schematic diagram of crosslinked species: IntraXL and InterXL/Inter2XL denote crosslinked species formed between α4 and α5 from either the same Noc subunit or from opposing subunits, respectively. Inter2XL represents a double crosslinking between α4 and α5′ and between α4′ and α5. *B*, crosslinking of Noc (E112C H143C) in the presence or absence of *NBS* and CTP and combinations thereof. Crosslinked species were resolved on an acrylamide gel and stained with Coomassie. Each crosslinking experiment was run in triplicate. *C*, crosslinking of *B. subtilis* Noc (E112C H143C) + CTP + *NBS* with an increasing concentration of BMOE. Crosslinked species were resolved on an acrylamide gel and stained with Coomassie. The top-most band appeared first as the concentration of BMOE is increasing from *left to right*, and thus it is thought to represent the singly crosslinked InterXL species. The doubly crosslinked Inter2XL presumably is more compacted and migrated faster than the InterXL on a denaturing acrylamide gel. Each crosslinking experiment was run in triplicate. BMOE, bismaleimidoethane; *NBS*, Noc-binding site; Noc, nucleoid occlusion protein; InterXL, Intermolecular singly crosslinked species; Inter2XL, Intermolecular doubly crosslinked species; IntraXL, Intramolecular crosslinked species.

5 mM magnesium chloride) for 10 min. Then, 20 mM of the crosslinking reagent (BMOE, dissolved in dimethyl sulfoxide) was added to the reaction to the final concentration of 2 mM. The mixture was incubated at room temperature for 5 min before the crosslinking reaction was quenched by SDS-PAGE loading dye + β-mercaptoethanol. Samples were heated to 90 °C for 10 min before being loaded on 4 to 12% Bis-Tris polyacrylamide gels (Thermo Fisher Scientific). Each experiment was triplicated. Polyacrylamide gels were stained in an InstantBlue Coomassie solution (Abcam) and band intensity was quantified using Image Studio-Lite (LICOR Biosciences). Raw gel images were deposited to the Mendeley repository: https://doi.org/10.17632/6sp26rm6zy.1.

Reconstitution of NBS *duplex DNA*

For X-ray crystallography: a 16-bp *NBS* DNA fragment (5′-TATTTCCC GGGAAATA-3′) (3.6 mM in buffer containing 10 mM Tris–HCl pH 8.0 and 250 mM sodium chloride) was heated to 98 °C for 5 min before being left to cool at room temperature overnight to form double-stranded *NBS* DNA (final concentration: 1.8 mM).

For HDX-MS experiment: a 22-bp *NBS* DNA fragment (5′-GGA TATTTCCC GGGAAATA TCC -3′) (100 μM in buffer containing 10 mM Tris–HCl pH 8.0 and 100 mM sodium chloride) was heated to 98 °C for 5 min before being left to cool at room temperature overnight to form double-stranded *NBS* DNA (final concentration: 50 μM).

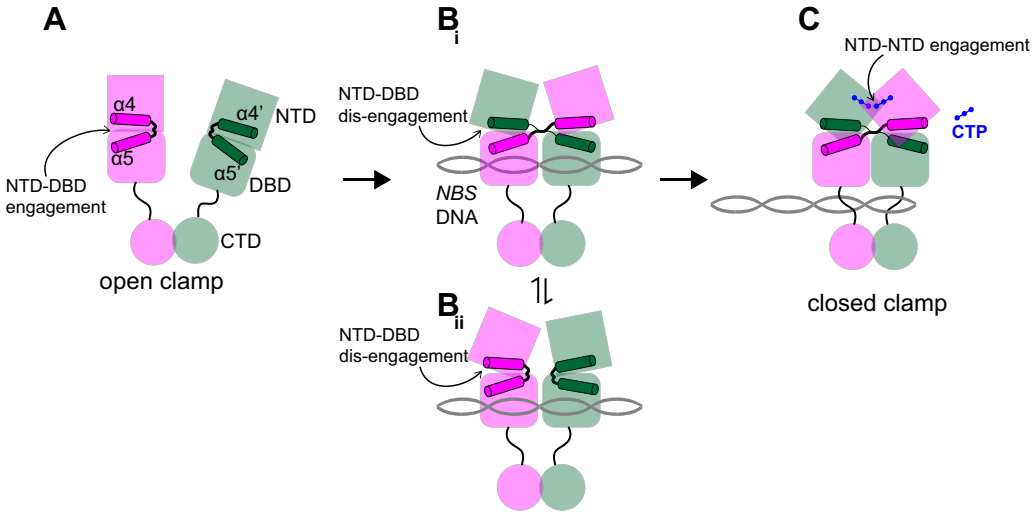

Figure 5. A possible model of different conformations of *Bacillus subtilis* Noc. In apo-Noc (*A*), helices α4 and α5 from the same Noc subunit (*magenta* or *dark green*) likely pack together, *i.e.*, the folding-back conformation (6). In *NBS*-bound Noc, helices α4 and α5 from the same Noc subunit are not packed together, instead α4 swings outwards to pack against α5′ from the adjacent Noc subunit, *i.e.*, the swinging-out conformation (B_i). As the result, the NTD and the DBD from the same Noc subunit disengage from each other, and there is no protein-protein contact between the majority of two adjacent NTDs of Noc. The proximity of adjacent Noc subunits and the restriction in movement by a DNA-bound DBD may increase the likelihood of helix swapping, this might contribute to promoting the NTD-NTD engagement upon CTP-binding (*C*). It is possible that helices α4 and α5 of *NBS*-bound Noc also take up a folding-back conformation (B_{ii}). In this case, NTDs of adjacent subunits of Noc likely adopt different orientations to avoid possible clashing between two adjacent protein subunits (15), the difference in orientations of opposing NTDs has been observed in the cocrystal structures of ParBΔCTD-*parS* from *Caulobacter crescentus* and *Helicobacter pylori* (11, 12). CTD, C-terminal domain; DBD, DNA-binding domain; *NBS*, Noc-binding site; Noc, nucleoid occlusion protein; NTD, N-terminal domain; ParB, Partitioning protein B; *parS*, Partitioning protein B binding site.

Protein crystallization, structure determination, and refinement

B. subtilis NocΔCTD-His_6 (∼10 mg/ml) was mixed with the 16-bp *NBS* DNA at a molar ratio of 1:1.2 (protein:DNA) in the gel filtration elution buffer (10 mM Tris–HCl pH 8.0, 250 mM sodium chloride). Crystallization screens were set up in sitting-drop vapor diffusion format in MRC2 96-well crystallization plates with drops comprised of 0.3 μl precipitant solution and 0.3 μl of protein and incubated at 293 K. After optimization of initial hits, the best crystals of the complex grew in a solution containing 17% (w/v) PEG3350, 0.25 M magnesium acetate, and 10% (v/v) sucrose. These were cryoprotected in the crystallization solution supplemented with 20% (v/v) glycerol and mounted in Litholoops (Molecular Dimensions) before flash-cooling by plunging into liquid nitrogen. X-ray data were recorded on beamline I04 at the Diamond Light Source (Oxfordshire) using an Eiger2 XE 16 M hybrid photon counting detector (Dectris), with crystals maintained at 100 K by a Cryojet cryocooler (Oxford Instruments). Diffraction data were integrated and scaled using DIALS (21) *via* the XIA2 expert system (22) and then merged using AIMLESS (23) to a resolution of 2.9 Å in space group $P2_12_12_1$ with cell parameters of a = 70.5, b = 99.3, c = 99.4 Å. Data collection statistics are summarized in Table 1. Analysis of the likely composition of ASU suggested that it contained two copies of the 29.5 kDa NocΔCTD monomer plus the 16-bp *NBS* duplex, giving an estimated solvent content of 51%.

The majority of the downstream analysis was performed through the CCP4i2 graphical user interface (24). For molecular replacement, a template was constructed from the structure of the *B. subtilis* Noc DBD complexed to an *NBS* duplex (PDB accession code 6Y93) (10). Initially, PHASER (25) was run using the protein and DNA components of this entry comprising two copies of the DBD and one DNA duplex, although the latter was truncated from a 22mer to a 16mer. This yielded a good solution and, in common with the template structure, the DNA formed a pseudocontinuous filament spanning the crystal due to base-pair stacking between DNA fragments in adjacent ASUs. However, there was only sufficient space to accommodate 15 bp per ASU within this filament. For the time being, the DNA model was truncated to the central 14 bp *NBS* site in COOT (26) before real space refining using "chain refine". The model was subsequently refined with REFMAC5 (27), using jelly body refinement giving R_{work} and R_{free} values of 0.363 and 0.404, respectively, to 2.9 Å resolution. Inspection of the electron density at this stage revealed evidence for the missing NTDs. A template for these was generated using SCULPTOR (28) from the *G. thermoleovorans* Noc structure (PDB accession code 7NFU) (6), where the corresponding domain shares 67% sequence identity with *B. subtilis*. After quickly tidying the output of the REFMAC5 job in COOT, this was put back into PHASER as a search model together with two copies of the NTD template. However, PHASER was only able to place one of the latter sensibly. After further jelly body refinement of this partial model (giving R_{work} and R_{free} values of 0.313 and 0.351, respectively, to 2.9 Å resolution), the electron density was inspected again in COOT, at which point it was possible to manually dock the missing domain into fragmented density. Following restrained refinement in REFMAC5, the density for the DNA was much clearer, enabling the missing DNA bases to be fitted. In one strand, the 5′ base was flipped out, and in the other, the 3′ base was flipped out, enabling a sticky-ended interaction (with a one-base overhang) between the duplexes in adjacent ASUs.

After further iterations of model building in COOT and restrained refinement in REFMAC5, the final model was produced with R_{work} and R_{free} values of 0.230 and 0.277, respectively, to 2.9 Å resolution. Refinement and validation statistics are summarized in Table 1.

Hydrogen-deuterium exchange coupled to mass spectrometry

HDX-MS experiments were carried out using an automated HDX robot (LEAP Technologies) coupled to an M-Class Acquity LC and HDX manager (Waters Ltd). Protein stocks were diluted to 10 μM in equilibration buffer (100 mM Tris, 150 mM sodium chloride, 5 mM calcium chloride, pH 8.0) prior to analysis. Twenty millimolars of 22-bp *NBS* DNA duplex were added to the stock sample where appropriate. Five microliters of the sample were added to 95 μl deuterated buffer (100 mM Tris, 150 mM sodium chloride, 5 mM calcium chloride, pH 8.0) and incubated at 4 °C for 0.5, 2, 10, or 60 min. Four different replicates were performed for each time point. Following the labeling reaction, samples were quenched by adding 75 μl of the labeled solution to 75 μl quench buffer (50 mM potassium phosphate, 0.05% n-Dodecyl-B-D-Maltoside which was pH adjusted to give a final quench pH of ∼ 2.5). Fifty microliters of the quenched sample were passed through a home-packed pepsin column using agarose immobilized pepsin (Thermo Fisher Scientific) at 40 μl min^{-1} (20 °C) and a VanGuard Pre-column Acquity UPLC BEH C18 (1.7 μm, 2.1 mm × 5 mm, Waters Ltd) for 3 min in 0.3% formic acid in water. The resulting peptic peptides were transferred to a C18 column (75 μm × 150 mm, Waters Ltd) and separated by gradient elution of 0 to 40% acetonitrile (0.1% v/v formic acid) in H_2O (0.3% v/v formic acid) over 12 min at 40 μl min^{-1}. Trapping and gradient elution of peptides was performed at 0 °C. The HDX system was interfaced to a Synapt G2Si mass spectrometer (Waters Ltd). High definition MSE and dynamic range extension modes (Data Independent Analysis coupled with ion mobility spectrometry separation) were used to separate peptides prior to collision induced dissociation fragmentation in the transfer cell. HDX data were analyzed using PLGS (v3.0.2) and DynamX (v3.0.0) software (https://www.waters.com/nextgen/us/en/products/informatics-and-software.html) supplied with the mass spectrometer. Restrictions for identified peptides in DynamX were as follows: minimum intensity: 10,000; minimum products per MS/MS spectrum: 3; minimum products per amino acid: 0.3; maximum sequence length: 18; maximum ppm error: 10; file threshold: 4/6. Following manual curation of the data, summary plots were generated using Deuteros 2.0 (29).

Data availability

The crystallographic model has been deposited in the Protein Data Bank as entry 7OL9. Raw gel images were deposited to the Mendeley repository: https://doi.org/10.17632/6sp26rm6zy.1.

Supporting information—This article contains supporting information.

Acknowledgments—This study was funded by the Royal Society University Research Fellowship Renewal (URF\R\201020 to T. B. K. L.) and BBSRC (BBS/E/J/000PR9791 to the John Innes Centre). We thank Diamond Light Source for access to beamline I04 under proposal MX18565 and Instruct-ERIC (PID: 14503) for access to the HDX-MS facility. The Waters MClass UPLC and HDX Manager, LEAP Sample Handling Robot and the Waters Synapt G2-Si were funded by the BBSRC (BB/M012573/1). We thank Clare Stevenson for assistance with X-ray crystallography. We thank S. Gruber, H. Antar, and T. McLean for discussions and comments on the manuscript.

Author contributions—K. V. S., A. S. B. J., and T. B. K. L. conceptualization; K. V. S., A. S. B. J., J. R. A., F. S., D. M. L., and T. B. K. L. data curation; K. V. S., A. S. B. J., J. R. A., D. M. L., and T. B. K. L. formal analysis; T. B. K. L. funding acquisition; K. V. S., A. S. B. J., J. R. A., and D. M. L. investigation; K. V. S., A. S. B. J., J. R. A., and D. M. L. methodology; F. S. and T. B. K. L. project administration; J. R. A., F. S., D. M. L., and T. B. K. L. resources; F. S., D. M. L., and T. B. K. L. supervision; K. V. S., A. S. B. J., J. R. A., and D. M. L. validation; K. V. S. and T. B. K. L. writing–original draft; K. V. S., A. S. B. J., J. R. A., F. S., D. M. L., and T. B. K. L. writing–review and editing.

Funding and additional information—K. V. S. is supported by Wellcome grant (221776/Z/20/Z). A. S. B. J.'s PhD studentship was funded by the Royal Society (RG150448).

Conflict of interest—The authors declare that they have no conflicts of interest with the contents of the article.

Abbreviations—The abbreviations used are: ASU, asymmetric unit; BMOE, bismaleimidoethane; CTD, C-terminal domain; DBD, DNA-binding domain; HDX-MS, Hydrogen-deuterium exchange coupled to mass spectrometry; InterXL, Intermolecular singly crosslinked species; Inter2XL, Intermolecular doubly crosslinked species; IntraXL, Intramolecular crosslinked species; *NBS*, Noc-binding site; Noc, Nucleoid occlusion protein; NTD, N-terminal domain; ParB, Partitioning protein B; *parS*, Partitioning protein B–binding site; PDB, Protein Data Bank.

References

1. Pang, T., Wang, X., Lim, H. C., Bernhardt, T. G., and Rudner, D. Z. (2017) The nucleoid occlusion factor Noc controls DNA replication initiation in Staphylococcus aureus. *PLoS Genet.* **13**, e1006908
2. Wu, L. J., and Errington, J. (2004) Coordination of cell division and chromosome segregation by a nucleoid occlusion protein in Bacillus subtilis. *Cell* **117**, 915–925
3. Rodrigues, C. D. A., and Harry, E. J. (2012) The min system and nucleoid occlusion are not required for identifying the division site in Bacillus subtilis but ensure its efficient utilization. *PLoS Genet.* **8**, e1002561
4. Yu, Y., Zhou, J., Gueiros-Filho, F. J., Kearns, D. B., and Jacobson, S. C. (2021) Noc corrals migration of FtsZ protofilaments during cytokinesis in Bacillus subtilis. *mBio* **12**, e02964–e03020
5. Adams, D. W., Wu, L. J., and Errington, J. (2015) Nucleoid occlusion protein Noc recruits DNA to the bacterial cell membrane. *EMBO J.* **34**, 491–501
6. Jalal, A. S., Tran, N. T., Wu, L. J., Ramakrishnan, K., Rejzek, M., Gobbato, G., *et al.* (2021) CTP regulates membrane-binding activity of the nucleoid occlusion protein Noc. *Mol. Cell* **81**, 3623–3636.e6
7. Soh, Y.-M., Davidson, I. F., Zamuner, S., Basquin, J., Bock, F. P., Taschner, M., *et al.* (2019) Self-organization of parS centromeres by the ParB CTP hydrolase. *Science* **366**, 1129–1133

8. Osorio-Valeriano, M., Altegoer, F., Steinchen, W., Urban, S., Liu, Y., Bange, G., *et al.* (2019) ParB-type DNA segregation proteins are CTP-dependent molecular switches. *Cell* **179**, 1512–1524.e15
9. Wu, L. J., Ishikawa, S., Kawai, Y., Oshima, T., Ogasawara, N., and Errington, J. (2009) Noc protein binds to specific DNA sequences to coordinate cell division with chromosome segregation. *EMBO J.* **28**, 1940–1952
10. Jalal, A. S., Tran, N. T., Stevenson, C. E., Chan, E. W., Lo, R., Tan, X., *et al.* (2020) Diversification of DNA-binding specificity by permissive and specificity-switching mutations in the ParB/Noc protein family. *Cell Rep.* **32**, 107928
11. Jalal, A. S., Tran, N. T., Stevenson, C. E., Chimthanawala, A., Badrinarayanan, A., Lawson, D. M., *et al.* (2021) A CTP-dependent gating mechanism enables ParB spreading on DNA. *Elife* **10**, e69676
12. Chen, B.-W., Lin, M.-H., Chu, C.-H., Hsu, C.-E., and Sun, Y.-J. (2015) Insights into ParB spreading from the complex structure of Spo0J and parS. *Proc. Natl. Acad. Sci. U. S. A.* **112**, 6613–6618
13. Leonard, T. A., Butler, P. J. G., and Löwe, J. (2004) Structural analysis of the chromosome segregation protein Spo0J from Thermus thermophilus. *Mol. Microbiol.* **53**, 419–432
14. Osorio-Valeriano, M., Altegoer, F., Das, C. K., Steinchen, W., Panis, G., Connolley, L., *et al.* (2021) The CTPase activity of ParB determines the size and dynamics of prokaryotic DNA partition complexes. *Mol. Cell* **81**, 3992–4007.e10
15. Antar, H., Soh, Y.-M., Zamuner, S., Bock, F. P., Anchimiuk, A., Rios, P. D. L., *et al.* (2021) Relief of ParB autoinhibition by parS DNA catalysis and recycling of ParB by CTP hydrolysis promote bacterial centromere assembly. *Sci. Adv.* **7**, eabj2854
16. Sievers, J., Raether, B., Perego, M., and Errington, J. (2002) Characterization of the parB-like yyaA gene of Bacillus subtilis. *J. Bacteriol.* **184**, 1102–1111
17. Jalal, A. S., Tran, N. T., and Le, T. B. (2020) ParB spreading on DNA requires cytidine triphosphate *in vitro*. *Elife* **9**, e53515
18. Balaguer, F. D. A., Aicart-Ramos, C., Fisher, G. L., de Bragança, S., Martin-Cuevas, E. M., Pastrana, C. L., *et al.* (2021) CTP promotes efficient ParB-dependent DNA condensation by facilitating one-dimensional diffusion from parS. *ELife* **10**, e67554
19. Walter, J.-C., Rech, J., Walliser, N.-O., Dorignac, J., Geniet, F., Palmeri, J., *et al.* (2020) Physical modeling of a sliding clamp mechanism for the spreading of ParB at short genomic distance from bacterial centromere sites. *iScience* **23**, 101861
20. Taylor, J. A., Seol, Y., Budhathoki, J., Neuman, K. C., and Mizuuchi, K. (2021) CTP and parS coordinate ParB partition complex dynamics and ParA-ATPase activation for ParABS-mediated DNA partitioning. *ELife* **10**, e65651
21. Winter, G., Waterman, D. G., Parkhurst, J. M., Brewster, A. S., Gildea, R. J., Gerstel, M., *et al.* (2018) Dials: implementation and evaluation of a new integration package. *Acta Crystallogr. D Struct. Biol.* **74**, 85–97
22. Winter, G. (2010) xia2: an expert system for macromolecular crystallography data reduction. *J. Appl. Cryst.* **43**, 186–190
23. Evans, P. R., and Murshudov, G. N. (2013) How good are my data and what is the resolution? *Acta Crystallogr. D Biol. Crystallogr.* **69**, 1204–1214
24. Potterton, L., Agirre, J., Ballard, C., Cowtan, K., Dodson, E., Evans, P. R., *et al.* (2018) CCP4i2: the new graphical user interface to the CCP4 program suite. *Acta Crystallogr. D Struct. Biol.* **74**, 68–84
25. McCoy, A. J., Grosse-Kunstleve, R. W., Adams, P. D., Winn, M. D., Storoni, L. C., and Read, R. J. (2007) Phaser crystallographic software. *J. Appl. Crystallogr.* **40**, 658–674
26. Emsley, P., and Cowtan, K. (2004) Coot: model-building tools for molecular graphics. *Acta Crystallogr. D Biol. Crystallogr.* **60**, 2126–2132
27. Murshudov, G. N., Vagin, A. A., and Dodson, E. J. (1997) Refinement of macromolecular structures by the maximum-likelihood method. *Acta Crystallogr. D Biol. Crystallogr.* **53**, 240–255
28. Bunkóczi, G., and Read, R. J. (2011) Improvement of molecular-replacement models with sculptor. *Acta Crystallogr. D Biol. Crystallogr.* **67**, 303–312
29. Lau, A. M., Claesen, J., Hansen, K., and Politis, A. (2021) Deuteros 2.0: peptide-level significance testing of data from hydrogen deuterium exchange mass spectrometry. *Bioinformatics* **37**, 270–272
30. Williams, C. J., Headd, J. J., Moriarty, N. W., Prisant, M. G., Videau, L. L., Deis, L. N., *et al.* (2018) MolProbity: more and better reference data for improved all-atom structure validation. *Protein Sci.* **27**, 293–315